HYBRID LATTICE BOLTZMANN/TAGUCHI OPTIMIZATION APPROACH FOR MAGNETOHYDRODYNAMIC NANOFLUID NATURAL CONVECTION IN A HEMISPHERE CAVITY

by

Javad ALINEJAD[*]

Department of Mechanical Engineering, Sari Branch,
Islamic Azad University, Sari, Iran

Original scientific paper
https://doi.org/10.2298/TSCI170509217D

In the present work, heat transfer optimization for natural convection with MHD flow in the hemisphere enclosure embedded with a vertical isothermal cylinder is investigated using Taguchi method. The simulations were planned based on Taguchi's L25 orthogonal array with each trial performed under different magnetic field, heat source aspect ratio and particle volume fraction of nanofluid. The thermal lattice Boltzmann based on D3Q19 methods was purposed to simulate the flow and thermal fields. Signal-to-noise ratios analyses were carried out in order to determine the effects of process parameters and optimal factor settings. The present results provide a good approximation for choosing effective parameters of designing the thermal system.

Key words: *Taguchi method, lattice Boltzmann, hemisphere enclosure, natural convection, magnetic field*

Introduction

The main idea of this study is simulation of MHD nanofluid heat transfer natural convection in a hemisphere cavity. This simulation is more important in industrial and technological applications including, electronic cooling [1], cooling of the reactors [2], heat and mass transfer processes in cryogenic fuel and vertical storage tanks [3]. In these works, the regimes of convective heat transfer in closed vertical volumes were analyzed in detail for the conditions when the thermal fluxes supplied to the liquid are uniformly distributed over the bottom and lateral surfaces. The spatial and temporal structure of convection at a sine distribution of the thermal flux on the lateral wall of the vertical cylinder was presented in [4]. The mathematical modeling of unsteady regimes of natural convection in a closed cylindrical region with a heat-conducting shell of finite thickness was carried out in [5]. Numerous studies of various convective flow based on entropy generation minimization are reported in literature [6-9]. Chatterjee and Chakraborty [6] examined the numerical formulation involving Second law of thermodynamics for entropy generation analysis of 3-D surface tension driven turbulent transport during laser materials processing. Esfahani and Alinejad [7] analyze the entropy generation due to conjugate natural convection in an enclosure. Transition criteria for entropy reduction of convective heat transfer from micro-patterned surfaces were reported by Naterer [8]. Entropy generation in micro-channel flow with presence of nanosized phase change particles was investigated by Alquaity *et al*. [9]. Recently lattice Boltzmann method (LBM) has been deveoped as a new tool for simulating the fluid-flow, heat transfer and other complicated physical phenom-

Author’s e-mail: Alinejad_javad@iausari.ac.ir

ena. Compared with the traditional CFD methods, the LBM is a meso-scale modeling method based on the particle kinematics. It has many advantages, such as simple coding, easy implementation of boundary conditions and fully parallelism. At present the applications of LBM [10-15] have achieved great success in multi-phase flow, chemical reaction flow, thermal hydrodynamics, suspension particle flow and MHD. Esfahani and Alinejad [16] conducted the simulation for viscous-fluid flow and conjugate heat transfer in a rectangular cavity by using LBM. D'Orazio *et al.* [17] and Shu *et al*. [18] performed the numerical calculations for the natural convection in a cavity. Moparthi *et al*. [19], Ajith *et al*. [20], and Das *et al*. [21] applied LBM to simulate the heat transfer problems. In these works, the significant parameters were studied in detail for choosing optimum parameters of different conditions. Several designs of experiments approaches have been applied to improve the efficiency of thermal system. A number of research studies have reported that the Taguchi design is an ideal method. The Taguchi approach is a simple and easy tool, which provides effective solutions on a design, as it emphasizes a mean performance value close to the target value. In this way, significant factors that have a significant impact on the experimental condition could be recognized and the optimal performance is determined [22-24]. We investigated the natural convection heat transfer of MHD flow in a 3-D cavity by means of Taguchi method. In this way, an L25 orthogonal array, including twenty five experiments for tree parameters with five levels, is used to optimize the processing factors. For this reason the thermal LBM with the Boussinesq approximation is employed to simulate natural convection. The effects of magnetic field, cylinder aspect ratio (AR), and particle volume fraction of nanofluid has been observed and analyzed in detail.

Lattice Boltzmann method

The LBM is particularly successful as a numerical method for solving the different fluid dynamic problems [25]. The LBM is derived from lattice gas methods as an explicit discretization of the Boltzmann equation in the phase space is considered. The LBM is a vigorous numerical method, based on the kinetic theory to simulate fluid-flow and heat transfer.

Unlike the classical macroscopic approach (Navier-Stokes) the lattice Boltzmann is a mesoscopic model to simulate flow field. In this approach, the fluid domain is made discrete in uniform Cartesian cells, each one of which holds a fixed number of distribution functions (DF) that represent the number of fluid particles moving in these discrete directions. Hence depending on the dimension and number of velocity directions, there are different models that can be used. The present study examined 3-D flow by using 3-D lattice with nineteen velocities (D3Q19 model). The velocities of the D3Q19 model are shown in fig. 1. The LB model used in the present work is the same as that employed in [26]. The DF are calculated by solving the lattice Boltzmann equation (LBE), which is a special discretization of the kinetic Boltzmann equation. After introducing Bhatnagar-Gross-Krook (BGK) approximation, the Boltzmann equation can be formulated [25]:

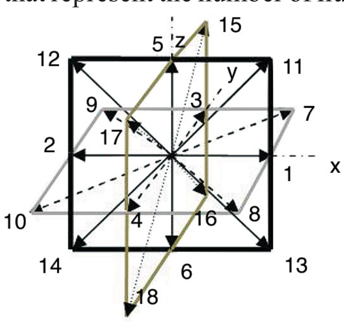

Figure 1. 3-D with 19-velocities lattice (D3Q19) model.

$$f_k(\mathbf{x} + \mathbf{c_k}\Delta t, t + \Delta t) = f_k(\mathbf{x},t) + \frac{\Delta t}{\tau}[f_k^{eq}(\mathbf{x},t) - f_k(\mathbf{x},t)] + \Delta t\mathbf{c_k}\mathbf{F_k} \tag{1}$$

where Δt, $\mathbf{c_k}$, τ, f_k^{eq}, $\mathbf{F_k}$ denote lattice time step, the discrete lattice velocity in direction k, the lattice relaxation time, the equilibrium DF, and the external force in the direction of the lattice velocity, respectively. The equilibrium distribution function for the D3Q19 velocity model is given by:

$$f_k^{\mathrm{eq}}(\mathbf{x},t) = \omega_k\rho\left[1+\frac{3\mathbf{c}_k\mathbf{u}}{c^2}+\frac{9(\mathbf{c}_k\mathbf{u})^2}{2c^2}-\frac{3\mathbf{u}^2}{2c^2}\right] \tag{2}$$

where

$$\omega_0=\frac{1}{3},\ \omega_k=\frac{1}{18}\ \text{for}\ k=1\text{-}6\ \text{and}\ \omega_k=\frac{1}{36}\ \text{for}\ k=7\text{-}18$$

In order to incorporate buoyancy force and magnetic forces in the model, the force term in eq. (1) needs to be calculated, in a vertical direction (z) as:

$$\begin{gathered}F=F_x+F_y+F_z\\
F_x=3\omega_k\rho\left(\frac{\mathrm{Ha}^2\mu}{L^2}\right)\{-\cos(\theta_z)\,[u\cos(\theta_z)+w\sin(\theta_z)\cos(\theta_x)]-\\
-\sin(\theta_z)\sin(\theta_x)\,[u\sin(\theta_z)\sin(\theta_x)-v\sin(\theta_z)\cos(\theta_x)]\}\\
F_y=3\omega_k\rho\left(\frac{\mathrm{Ha}^2\mu}{L^2}\right)\{-\sin(\theta_z)\cos(\theta_x)[\mathrm{u}\sin(\theta_z)\sin(\theta_x)-v\sin(\theta_z)\cos(\theta_x)]-\\
-\cos(\theta_z)\,[v\cos(\theta_z)-w\sin(\theta_z)\sin(\theta_x)]\}\\
F_z=3\omega_k\rho \mathrm{g}_z\beta\theta+3\omega_k\rho\left(\frac{\mathrm{Ha}^2\mu}{L^2}\right)\{\sin(\theta_z)\sin(\theta_x)[v\cos(\theta_z)-w\sin(\theta_z)\sin(\theta_x)]-\\
-\sin(\theta_z)\cos(\theta_x)[u\cos(\theta_z)-w\sin(\theta_z)\cos(\theta_x)]\}\end{gathered}\tag{3}$$

where θ_z and θ_x are the orientation of the magnetic field with z and x axis, respectively. u, v, w are velocity components in the x-, y-, and z-direction. The macroscopic fluid densities and velocities are computed:

$$\rho=\Sigma_{k=0}^{18}f_k,\ \mathbf{u}=\frac{1}{\rho}\Sigma_{k=0}^{18}f_k\mathbf{c}_\mathbf{k} \tag{4}$$

For the temperature field the g distribution is:

$$g_k(\mathbf{x}+\mathbf{c}_k\Delta t,t+\Delta t)=g_k(\mathbf{x},t)+\frac{\Delta t}{\tau_g}[g_k^{\mathrm{eq}}(\mathbf{x},t)-g_k(\mathbf{x},t)] \tag{5}$$

For the D3Q19 model, the equilibrium energy DF can be defined:

$$g_0^{\mathrm{eq}}=-\frac{T}{2}\frac{u^2}{c^2} \tag{6}$$

$$g_{1-6}^{\mathrm{eq}}=\frac{T}{18}\left[1+\frac{c_k\mathbf{u}}{c^2}+\frac{9(c_k\mathbf{u})^2}{2c^2}-\frac{3\mathbf{u}^2}{2c^2}\right] \tag{7}$$

$$g_{7-18}^{\mathrm{eq}}=\frac{T}{36}\left[2+4\frac{\mathbf{c}_k\mathbf{u}}{c^2}+\frac{9(\mathbf{c}_k\mathbf{u})^2}{2c^4}-\frac{3\mathbf{u}^2}{2c^2}\right] \tag{8}$$

The temperature field is computed as:

$$T=\sum_{k=0}^{18} \tag{9}$$

Lattice Boltzmann model for nanofuid

In order to simulate the nanofluid by the LBM, because of the interparticle potentials and other forces on the nanoparticles, the nanofluid behaves differently from the pure liquid from the mesoscopic point of view and is of higher efficiency in energy transport as well as better stabilization than the common solid-liquid mixture. For pure fluid in absence of nanoparticles in the enclosures, the governing equations are eqs. (1)-(9). However for modeling the nanofluid because of changing in the fluid thermal conductivity, density, heat capacitance and thermal expansion, some of the governed equations should be changed. The thermal diffusivity is written:

$$\alpha_{\mathrm{nf}}=\frac{k_{\mathrm{nf}}}{(\rho c_p)_{\mathrm{nf}}} \tag{10}$$

The effect of density at reference temperature is given by:

$$\rho_{\mathrm{nf}}=(1-\phi)\,\rho_{\mathrm{f}}+\phi\rho_{\mathrm{s}} \tag{11}$$

The heat capacitance and thermal expansion of nanofluid can be given as [21]:

$$(\rho c_p)_{\mathrm{nf}} = (1 - \phi)(\rho c_p)_{\mathrm{f}} + \phi\,(\rho c_p)_{\mathrm{s}} \tag{12}$$

$$\beta_{\mathrm{nf}} = (1 - \phi)\,\beta_{\mathrm{f}} + \phi\beta_{\mathrm{s}} \tag{13}$$

The viscosity of the nanofluid containing a dilute suspension of small rigid spherical particles is given by Brinkman model [28]:

$$\mu_{\mathrm{nf}} = \frac{\mu_{\mathrm{f}}}{(1 - \phi)^{2.5}} \tag{14}$$

The effective thermal conductivity of the two component entities of spherical-particle suspension was introduced by Chon *et al*. [29]:

$$\frac{k_{\mathrm{nf}}}{k_{\mathrm{f}}} = 1 + 64.7\,\phi^{0.764}\left(\frac{d_{\mathrm{f}}}{d_{\mathrm{s}}}\right)^{0.369}\left(\frac{k_{\mathrm{f}}}{k_{\mathrm{s}}}\right)^{0.7476}\mathrm{Pr}_T\mathrm{Re}_T^{\,1.2321} \tag{15}$$

Where Pr_T and Re_T are given:

$$\mathrm{Pr}_T = \frac{\mu_{\mathrm{f}}}{\rho_{\mathrm{f}}\alpha_{\mathrm{f}}},\ \mathrm{Re}_T = \frac{\rho_{\mathrm{f}} k_{\mathrm{b}} T}{3\pi\mu_{\mathrm{f}}^2 l_{\mathrm{f}}} \tag{16}$$

where l_{f} is the mean path of the fluid particle (17 nm) and k_b is the Boltzmann constant. It should be mentioned that, this model is based on experimental measurements of Chon *et al*. [29] for Al_2O_3 suspension in water and include the nanoparticles size and the work temperature effects. However, Minsta *et al*. [30] found that this model is suitable for thermal conductivity prediction of both Al_2O_3 and CuO nanoparticles by experimental test.

Nusselt number

Heat transfer between hot and cold walls was computed by local and mean Nusselt number which is given:

$$\mathrm{Nu}_l = \frac{-1}{\theta_{\mathrm{m}}}\left.\frac{\partial\theta}{\partial n}\right|_{\mathrm{wall}},\ \theta_{\mathrm{m}} = \frac{T - T_{\mathrm{c}}}{T_{\mathrm{h}} - T_{\mathrm{c}}} \tag{17}$$

$$\mathrm{Nu}_{\mathrm{m}} = \frac{1}{l}\int_0^l \mathrm{Nu}_l\,\mathrm{d}x \tag{18}$$

Turbulent natural convection modeling

In the present study the thermal lattice Boltzmann based on D3Q19 methods without any turbulent models was purposed to simulate the flow and thermal fields. For stable and convergence solution in natural convection the maximum velocity should not exceed the critical magnitude ($u_{\max} \leq 0.1$) and the relaxation time must be as large as possible. For these reasons we use the scale analysis of the natural convection boundary layer to find the suitable relaxation time:

$$\text{For Pr} < 1\text{: } u_{\max} \sim \frac{\vartheta}{H}\left(\frac{\mathrm{Ra}}{\mathrm{Pr}}\right)^{1/2} \tag{19}$$

$$\text{For Pr} > 1\text{: } u_{\max} \sim \frac{\vartheta}{H}\left(\frac{\mathrm{Ra}^{1/2}}{\mathrm{Pr}}\right) \tag{20}$$

Proportionalities (19) and (20) can be converted to equalities using constants sc_1 and sc_2. These constants could be calculated for different geometries by solving the problem in a more stable condition. It should be noted that sc_1 and sc_2 are less than unity:

$$\text{For Pr} < 1\text{: } u_{\max} = sc_1\frac{\vartheta}{H}\left(\frac{\mathrm{Ra}}{\mathrm{Pr}}\right)^{1/2} \tag{21}$$

$$\text{For Pr} > 1\text{: } u_{\max} = sc_2\frac{\vartheta}{H}\left(\frac{\mathrm{Ra}^{1/2}}{\mathrm{Pr}}\right) \tag{22}$$

Substituting $u_{\max} \le 0.1$ and solving for ϑ:

$$\text{For Pr} > 1: \vartheta \le \frac{0.1}{sc_1}\left(\frac{\text{Pr}}{\text{Ra}}\right)^{1/2} H \tag{23}$$

$$\text{For Pr} > 1: \vartheta \le \frac{0.1}{sc_2}\left(\frac{\text{Pr}}{\text{Ra}^{1/2}}\right) H \tag{24}$$

By these equations the relaxation times calculated:

$$\text{For Pr} < 1: \begin{cases} \tau \le \left(\dfrac{0.1}{sc_1}\right)\left(\dfrac{1}{c_s^2 \Delta t}\right)\left(\dfrac{\text{Pr}}{\text{Ra}}\right)^{1/2} H + 0.5 \\ \tau_g \le \left(\dfrac{0.1}{sc_1}\right)\left(\dfrac{1}{c_s^2 \Delta t}\right)\left(\dfrac{1}{\text{RaPr}}\right)^{1/2} H + 0.5 \end{cases} \tag{25}$$

$$\text{For Pr} > 1: \begin{cases} \tau \le \left(\dfrac{0.1}{sc_2}\right)\left(\dfrac{1}{c_s^2 \Delta t}\right)\left(\dfrac{\text{Pr}}{\text{Ra}^{1/2}}\right) H + 0.5 \\ \tau_g \le \left(\dfrac{0.1}{sc_2}\right)\left(\dfrac{1}{c_s^2 \Delta t}\right)\left(\dfrac{1}{\text{Ra}^{1/2}}\right) H + 0.5 \end{cases} \tag{26}$$

Physical model

The physical geometry considered in this study is shown in fig. 2. Figure 2(a) shows the schematic diagrams of the benchmark problem. In the present study, we consider the natural convection of a viscous incompressible fluid in a hemispherical enclosure, fig. 2(b), in the presence of a local energy source with constant temperature, T_c. When doing numerical simulation it was assumed that the thermophysical properties of the material are temperature-independent. In the present study the flow is bounded by an enclosure with the geometric set-up, $D = 5\,(hd)^{1/2}$ where denote the cavity diameter and the heat source dimension, respectively.

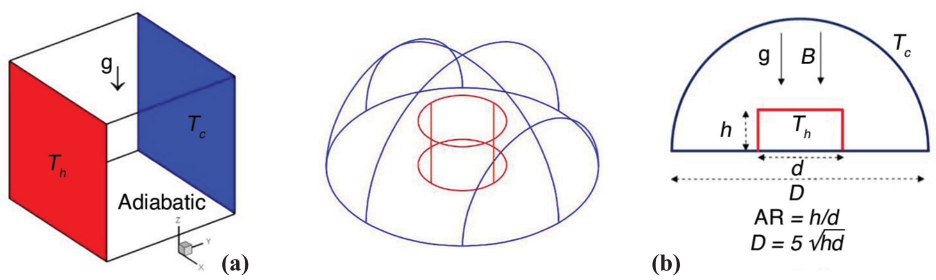

Figure 2. Schematic diagrams of the benchmark problem (a), and present study (b).

Curved boundary treatment

Consider fig. 3(a) is a part of arbitrary curved wall geometry, where the black small circles, x_w, the open circles, x_f, and the grey circles, x_b, represent the boundary, the fluid region and the solid region nodes, respectively. In the boundary condition $\tilde{f}(x_b,t)$ is needed to perform the streaming steps on fluid nodes x_f. The fraction of an intersected link in the fluid region Δ is defined by:

$$\Delta = \frac{\| x_f - x_w \|}{\| x_f - x_b \|} \tag{27}$$

The standard (half-way) bounce back no-slip boundary condition always assumes a delta value of 0.5 to the boundary wall, fig. 3(b). Due to the curved boundaries, delta values in the interval of (0, 1) are now possible. Figure 3(c) shows the bounce back behavior of a surface with a delta value smaller than 0.5 and fig. 3(d) shows the bounce back behavior of a wall with delta bigger than 0.5. In all three cases, the reflected distribution function $f\tilde{\alpha}\,(x, t + \Delta t)$ at x_f is unknown.

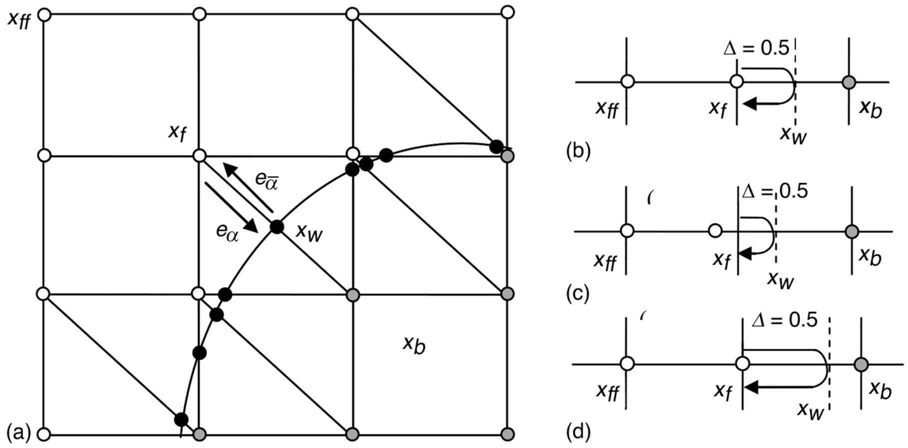

Figure 3. Layout of the regularly spaced lattices and curved wall boundary; (a) overall view, (b) Δ = 0.5, (c) Δ < 0.5, (d) Δ > 0.5

Since the fluid particles in the LBM are always considered to move one cell length per time step, the fluid particles would come to rest at an intermediate node x_i. In order to calculate the reflected distribution function in node x_f an interpolation scheme has to be applied. For treating velocity field in curved boundaries, the method is based on the method reported in [28]. To calculate the distribution function in the solid region $\tilde{f}\bar{\alpha}\,(x_b,t)$ based upon the boundary nodes in the fluid region, the bounce-back boundary conditions combined with interpolations including a one-half grid spacing correction at the boundaries. Then the Chapman-Enskog expansion for the post-collision distribution function is conducted:

$$\tilde{f}_{\bar{\alpha}}\,(x_b,t+\Delta t) = (1-\lambda)\,\tilde{f}_\alpha(x_f,t+\Delta t) + \lambda f_\alpha^0\,(x_b,t+\Delta t) - 2\,\frac{3}{c^2}\omega_\alpha\,\rho\,(x_f\,,t+\Delta t)\;e_\alpha{\cdot}u_w \tag{28}$$

where

$$f_\alpha^0\,(x_b,t+\Delta t) = f_\alpha^{\mathrm{eq}}(x_f,t+\Delta t) + \frac{3}{c^2}w_\alpha\,\rho\,(x_f\,,t+\Delta t)\;e_\alpha(u_{bf}-u_f) \tag{29}$$

$$u_{bf} = u_{ff}\,,\ \lambda = \frac{2\Delta-1}{\tau_m-2}\ \text{if}\ \ 0<\Delta\leq\frac{1}{2} \tag{30a}$$

$$u_{bf} = \left(1-\frac{3}{2\Delta}\right)u_f + \frac{3}{2\Delta}u_w,\ \ \lambda = \frac{2\Delta-1}{\tau_m+\frac{1}{2}}\ \text{if}\ \ \frac{1}{2}<\Delta\leq 1 \tag{30b}$$

Grid independency

For grid independency, the average Nusselt number was calculated at high Rayleigh numbers for different grid points. As seen in tab.1 for grid points passing from 80 × 80 × 80 to 100 × 100 × 100 for Ra = 10^6 and from 150 × 150 × 150 to 200 × 200 × 200 for 10^9, respectively, no considerably change in the average Nusselt number is observed (maximum variation is less than 0.3%). According to the tab. 1, the 100 × 100 × 100 grid points was used for Ra ≤ 10^8 and 200 × 200 × 200 grid points was used only for Ra = 10^9.

Table 1. Effect of spatial resolution on the mean Nusselt number at different Rayleigh number

Mesh size	40 × 40 × 40	80 × 80 × 80	100 × 100 × 100	150×150×150	200 × 200 × 200
Ra = 10^6	8.815	8.843	8.845	–	–
Ra = 10^9	–	–	52.374	53.116	53.264

Code validation

The numerical simulation was done by an in-house code written in FORTRAN, using LBM. Numerical investigations were carried out for the following values of dimensionless Rayleigh number, $103 < \mathrm{Ra} < 109$. The influence of the main parameters characterizing the process was analyzed. The obtained results are compared with the previous 2-D and 3-D simulations of turbulent natural convection in a square cavity [31-34]. The comparison of streamlines, isotherms and mean Nusselt number at the interface between the solid wall and gaseous cavity with previous work at different Rayleigh numbers illustrates a fine agreement that has been obtained (fig. 4 and tab. 2). The isotherm lines vortex indicates a change in the dominant

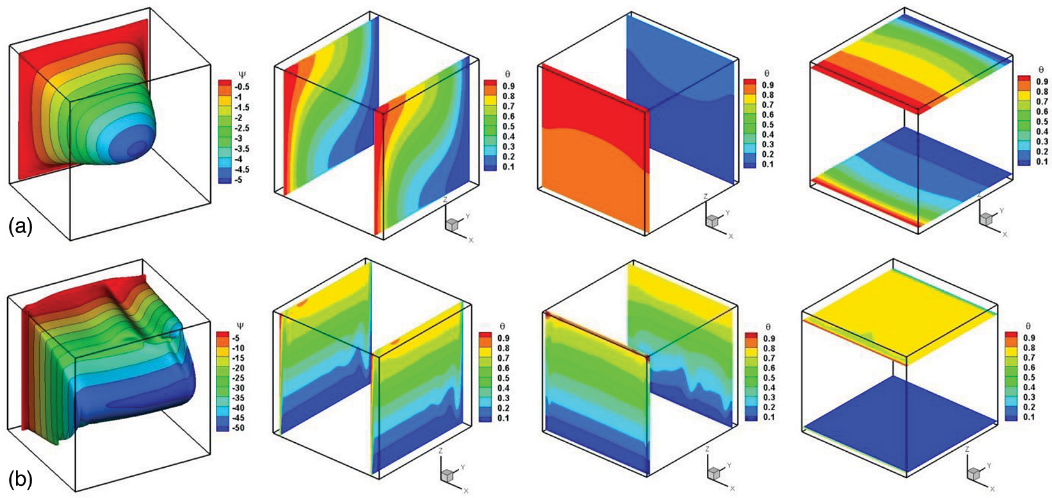

Figure 4. Streamlines and isotherms at (a) Ra = 10^4, (b) Ra = 10^8

heat transfer mechanism with Rayleigh number. For low Rayleigh number, isotherms are aligned with the temperature constant walls and slightly deviated by the flow, and the heat is transferred mainly by heat conduction. As Rayleigh number increases, the controlling heat transfer mechanism changes from conduction to convection, the shape of isotherms begins to bend in the bulk region. The isotherm lines become flat in the central region of the cavity. These lines are vertical only in thin boundary-layers near the hot and cold walls and the fluid is thermally arranged in different layers. In other words, the isotherms become horizontal in the cavity. Observing the streamlines patterns reveals wavy disturbances occurrence close to the horizontal adiabatic boundary specially at upper-left and bottom right corners. These patterns intensify by increasing Rayleigh number and finally eddies are developed. The temperature field becomes more and more stratified. The isotherms near the hot wall stretch upward as a result of the warm

Table 2. Comparison of mean Nusselt number at mid-plane (x = 0.5) with the bench-mark data

Rayleigh number	10^3	10^4	10^5	10^6	10^7	10^8	10^9
Present study	1.113	2.231	4.520	8.845	16.499	29.590	53.264
[31]	1.108	2.252	4.596	8.822	16.424	29.094	49.110
[32]	1.121	2.286	4.546	8.652	16.790	30.506	57.350
[33]	1.114	2.245	4.510	8.806	–	30.1	54.4
[34]	1.070	2.057	4.359	8.794	17.267	–	–

fluid wake. The streamlines on the 3-D cavity show that the fluid has a tendency to flow to the cavity center in the *X*-direction. This observation cannot be distinguished in 2-D simulation. Finally, it should be noted that there is an excellent agreement between the present results and the benchmark LBM solution by Du and Liu [31] and Dixit and Babu [32] for all values of Rayleigh number (maximum difference is less than 8%), as well as with the CFD 2-D solutions by Barakos and Mitsoulis [33] and 3-D solutions by Bocu and Altac [34] (maximum difference is less than 4%).

Results and discussion

The effect of nanofluid and different aspect ratio

Figure 6 shows the average Nusselt number at $Gr = 2 \cdot 10^5$ for different volume fractions and Hartmann number. From this figure, it can be found that, as the solid volume fraction increases from 0% to 5%, the Nusselt number distribution along the heated surface increases. For Hartmann numbers, it is obvious that the Nusselt number along the hot wall decreases, because by increasing the Hartmann number, the effect of convection reduces and the dominant heat transfer mechanism is conduction.

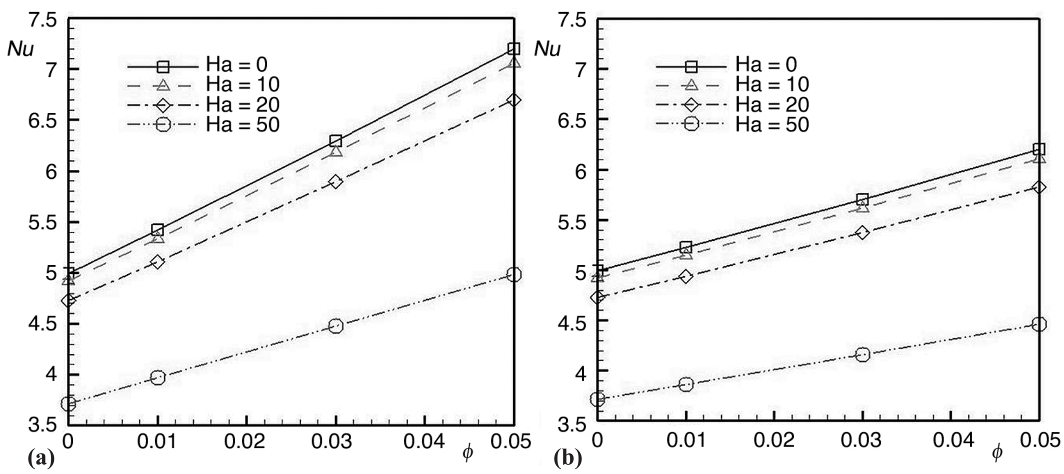

Figure 6. Average Nusselt number for different volume fraction of (a) CuO-water (b) Al_2O_3-water

The streamlines, fig. 7(a), and isotherms, fig. 7(b), are observed in fig. 7. Illustrative figures are shown at $Gr = 2 \cdot 10^5$ and different AR (AR = *a/b*) in various cases. As a result of the buoyancy effect, the fluid from the hot cylinder in the cavity rises and along the cold hemispherical wall descends. These flow circulations create many similar rolls in the cavity. By the natural convection mechanism the heat transports from the heated wall to the cold ambient.

Application of the Taguchi method

Taguchi method is proposed by Taguchi in 1960s. This method is widely applied for improving industrial product quality greatly [35, 36]. In addition to this, low trial numbers, obtaining the effects of process parameters on quality characteristics and their optimum levels has easily increased its popularity. In the present study, the effects of magnetic field, heat source AR and particle volume fraction of nanofluid on heat transfer rate (Nu) have been determined and optimum factor levels have been obtained by analyzing Taguchi method. To get more accurate in terms of the heat transfer rate, the Nusselt numbers over the wall of the cylinder for various designated trial have been calculated. The specified factors and their levels are depicted in and tab. 3.

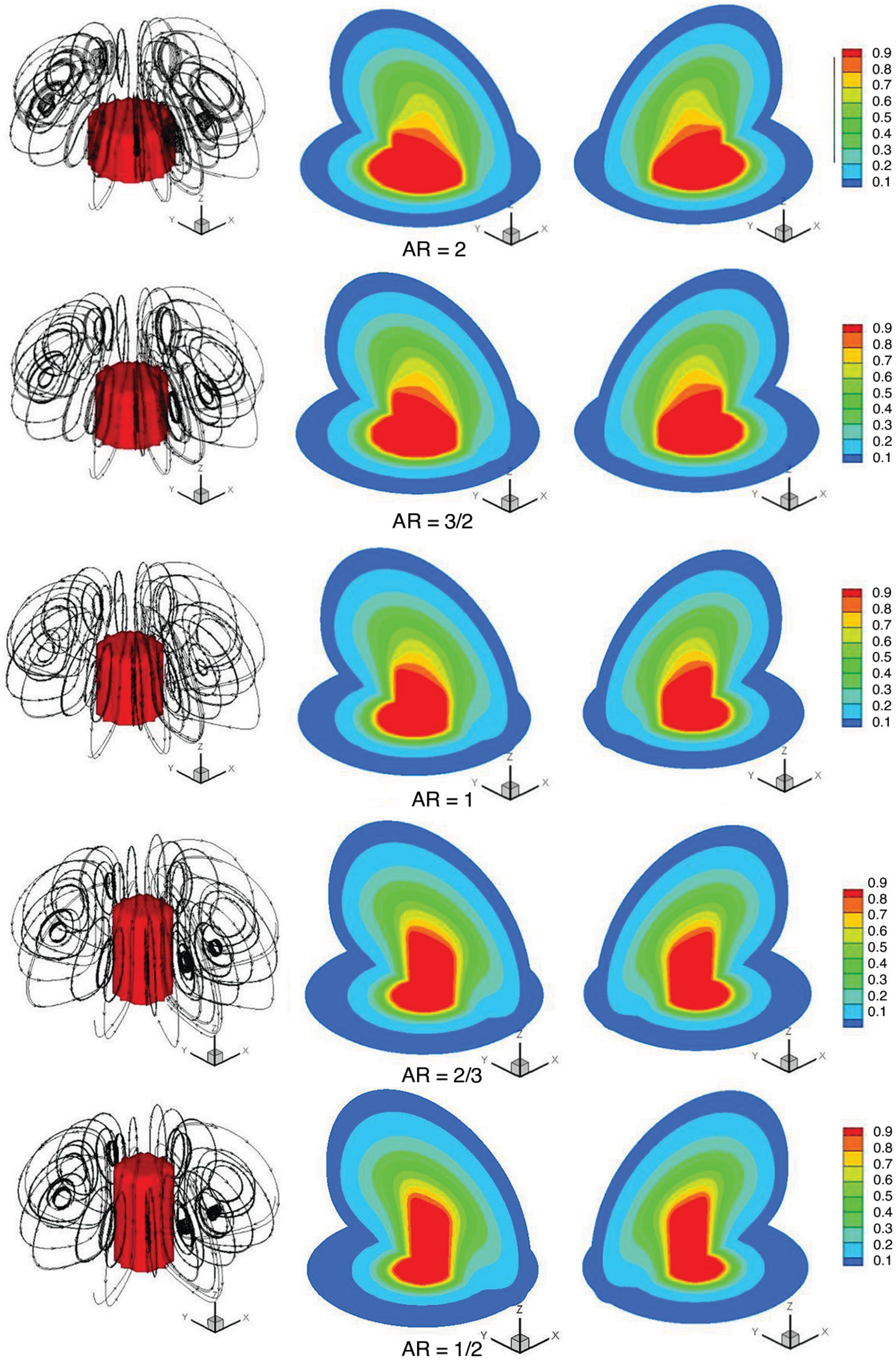

Figure 7. Streamlines and isotherms for different AR of heat source at Ra = 10^5, Ha = 50

Table 3. Factors and their levels of simulation

Factors	Heat source AR					Magnetic field Ha					Nanofluid volume fraction (ϕ)				
											CuO		Water	Al_2O_3	
Levels	1/2	2/3	1	3/2	2	10	20	30	40	50	0.05	0.02	–	0.02	0.05
No.	1	2	3	4	5	1	2	3	4	5	1	2	3	4	5

The number of simulation can be reduced by means of Taguchi technique, based on orthogonal arrays. This method uses the special design of orthogonal arrays to learn the whole parameters space with small number of experiments. In the present study, an L25 orthogonal array by three factors with five levels is chosen as shown in tab. 4. Taguchi method employs a signal-to-noise (S/N) ratio to measure the present variation. Also, in calculation procedure the effect of different control factors and their interaction was assumed. In Taguchi designs, a measure of robustness used to identify control factors that reduce variability in a product or process by minimizing the effects of uncontrollable factors (noise factors). The definition of S/N ratio differs according to an objective function, *i.e.*, a characteristic value. There are three kinds of characteristic value: Nominal is Best (NB: n = 10 Log10 [square of mean/variance]), Smaller is Better (SB: n = –10 Log10 [mean of sum of squares of measured data]), and Larger is Better (LB: n = –10 Log10 [mean of sum squares of reciprocal of measured data]). As the maximum heat transfer rate (Nu) is major goal in present study, LB is chosen as a characteristic value. The S/N ratios plots for different factors are given in fig. 8. Higher values of the S/N ratios identify control factor settings that minimize the effects of the noise factors. As a result, the higher values of S/N for optimum settings of control factors maximizing the Nusselt number are AR = 2, Ha =10, and ϕ = 0.05 (CuO).

Table 4. The L25 Orthogonal array with control factors

Trial No.	1	2	3	4	5	6	7	8	9	10	11	12	13
AR	1	1	1	1	1	2	2	2	2	2	3	3	3
Ha	1	2	3	4	5	1	2	3	4	5	1	2	3
ϕ	1	2	3	4	5	2	3	4	5	1	3	4	5
Nu	1.893	1.475	1.204	1.233	1.291	1.536	1.273	1.326	1.409	1.515	1.316	1.399	1.516
Trial No.	14	15	16	17	18	19	20	21	22	23	24	25	
AR	3	3	4	4	4	4	4	5	5	5	5	5	
Ha	4	5	1	2	3	4	5	1	2	3	4	5	
ϕ	1	2	4	5	1	2	3	5	1	2	3	4	
Nu	1.658	1.273	1.465	1.627	1.828	1.406	1.146	1.743	2.007	1.549	1.264	1.322	

The maximum Nusselt number occurs at this optimum setting because of the nature of fluid-flow in free convection. The fluid in cavity becomes warm and upward flow stream along the heat source. The curved cold wall of the cavity leads the fluid-flow to the bottom wall slowly. Finally, it should be noted that choosing the tall cylinder shape for the heat source terminates to increase the heat transfer rate. The final step in verifying results based on Taguchi design is the confirmation test. Numerical results indicate that the Nusselt number in the optimum case is equal to 2.059. It can be concluded that Taguchi method achieves the statistical assessment of maximum heat transfer rate of natural convection in a hemispherical enclosure embedded with vertical isothermal cylinder.

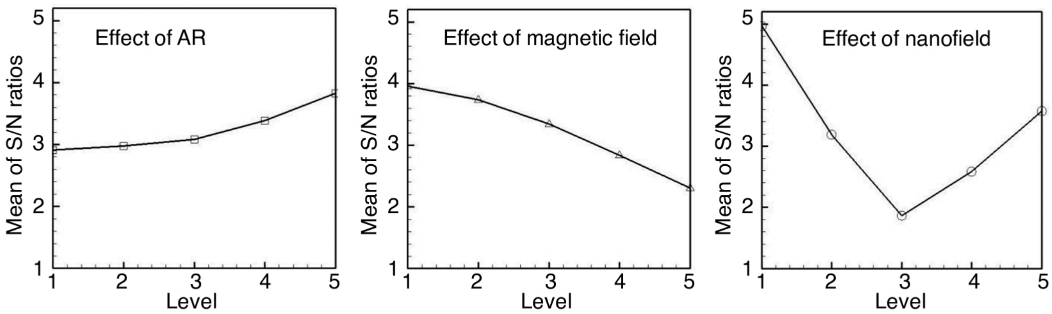

Figure 8. The S/N ratios plots for different factors

Conclusions

In this article, the effects of different parameters on natural convection heat transfer in a hemispherical cavity are investigated through Taguchi method. Achievement the maximum heat transfer rate by optimum condition is the practical benefit of this study. The simulation is numerically predicted by using LBM. The experiments are planned by means of Taguchi's L25 orthogonal array under different conditions of magnetic field, heat source aspect ratio, and particle volume fraction of nanofluid. In conclusion, some of the main points are briefly remarked as follows.

- Using LBM for natural convection simulation has a simple calculation procedure in comparison with CFD method.
- Present study show in 3-D natural convection, fluid have tendency to flow in the x-direction of cavity center.
- Based on the S/N ratio plots, all control factors (Hartman number, AR, ϕ, have significant effect on the objective function.
- The optimum settings of control factors are the heat source aspect ratio AR = 2, magnetic field Ha = 10, and the particle volume fraction of nanofluid $\phi = 0.05$ (CuO).
- Confirmation test verify the maximum heat transfer rate of natural convection in a cubic cavity can be predicted by Taguchi method with sufficient accuracy.

Nomenclature

B – magnetic field, [T]
$\mathbf{c_k}$ – discrete lattice velocity in direction, [k]
$\mathbf{F_k}$ – external force in direction of lattice velocity, [N]
f_k, g_k – distribution functions
f_k^{eq}, g_k^{eq} – equilibrium distribution functions
g – gravitational acceleration, [ms^{-2}]
H – enclosure height [m]
k – thermal conductivity [Wm^{-1}K^{-1}]
T_h – hot temperature, [K]
T_c – cold temperature, [K]
u,v,w – velocities, [ms^{-1}]
x,y,z – co-ordinates, [m]
Nu_l – local Nusselt number, [$= (\partial\theta/\partial n)/\theta_m$]
Nu_m – mean Nusselt number, [$= (\int_0^l \mathrm{Nu}_l\, dx/l$]
Pr – prandtl number, [υ,α]
Ra – rayleigh number, [$g\beta\Delta T H^3/\alpha\upsilon$]
Gr – grashof number, [$g\beta\Delta T H^3/\upsilon^2$]
Ha – hartmann number, [$BH/\sqrt{\sigma/\rho_\upsilon}$]

Greek symbols

α – thermal diffusivity [m^{2}s^{-1}]
β – thermal expansion coeficient [K^{-1}]
υ – kinematic viscosity [m^{2}s^{-1}]
μ – dynamic viscosity [kg m^{-1}s^{-1}]
ρ – fluid density [kg m^{-3}]
θ_m – dimensionless temperature [$T - T_c/T_h - T_c$]
τ – relaxation time for flow field
τ_g – relaxation time for thermal field

Subscript

f – fluid
max – maximum
nf – nanofluid
s – solid

Refrences

[1] Samadiani, E., *et al*., The Thermal Design of a Next Generation Data Center: A Conceptual Exposition, *Journal of Electronic Packaging*, *130* (2008), 4, pp. 1104-1112
[2] Karthikeyan, S., *et al*., Effect of Turbulent Natural Convection on Sodium Pool Combustion in the Steam Generator Building of a Fast Breeder Reactor, *Nuclear Engineering and Design*, *239* (2009), 12, pp. 2992-3002
[3] Rodriguez, I., *et al.*, Unsteady Numerical Simulation of the Cooling Process of Vertical Storage Tanks Under Laminar Natural Convection, *International Journal of Thermal Sciences*, *48* (2009), 4, pp. 708-721
[4] Moiseeva, L. A., Cherkasov, S. G., Mathematical Modeling of Natural Convection in a Vertical Cylindricaltank with Alternating-Sign Heat Flux Distribution on the Wall, *Fluid Dynamics*, *31* (1996), 2, pp. 218-223
[5] Sheremet, M. A., Unsteady Conjugate Thermogravitational Convection in a Cylindrical Region with Local Energy Source, *Thermophysics and Aeromechanics*, *18* (2011), 3, pp. 447-458
[6] Chatterjee, D., Chakraborty, S., Entropy Generation Analysis of Turbulent Transport in Laser Surface Alloying process, *Materials Science and Technology*, *22* (2006), 6, pp. 627-633
[7] Esfahani, J. A., Alinejad, J., Entropy Generation of Conjugate Natural Convection in Enclosures: the Lattice Boltzmann Method, *Journal of Thermophysics and Heat Transfer*, *27* (2013), 3, pp. 498-505
[8] Naterer, G., Transition Criteria for Entropy Reduction of Convective Heat Transfer from Micropatterned Surfaces, *Journal of Thermophysics and Heat Transfer*, *22* (2008), 2, pp. 271-280
[9] Alquaity, A. B. S., *et al*., Entropy Generation in Microchannel Flow with Presence of Nanosized Phase Change Particles, *Journal of Thermophysics and Heat Transfer*, *26* (2012), 1, pp. 134-140
[10] Nemati, H., *et al*., Latitice Boltzmann Simulation of Nanofluid in Lid-Driven Cavity, *International Communications in Heat and Mass Transfer*, *37* (2010), 10, pp. 1528-1534
[11] Fattahi, E., *et al*., Lattice Boltzmann Simulation of Natural Convection Heat Transfer in Eccentric Annulus, *International journal of thermal sciences*, *49* (2012), 12, pp. 2353-2362
[12] Fattahi, E., *et al*.., Lattice Boltzmann Simulation of Natural Convection Heat Transfer in Nanofluids, *International Journal of Thermal Sciences*, *52* (2012), Feb., pp.137-144
[13] MenduSubrahmanyam, S., *et al.*, Simulation of Natural Convection of Nanofluids in a Square Enclosure Embedded with Bottom Discrete Heater, *Thermal Science*, *22* (2018), 6B, pp. 2771-2781
[14] Shouguang, Y., *et al*., Simulation of Flow Boiling of Nanofluid in Tube Based on LBM, *Thermal Science*, *23* (2019), 1, pp. 159-168
[15] Sajjadi, H., Kefayati, R., Lattice Boltzmann Simulation of Turbulent Natural Convection in Tall Enclosures, *Thermal Science*, *19* (2015), 1, pp. 155-166
[16] Esfahani, J. A., Alinehad, J., Latitice Boltzmann Simulation od Viscous-Fluid Flow and Conjugate Heat Transfer in a Rectangular Cavity with a Heated Moving Wall, *Thermophysics and Aeromechanics*, *20* (2013), 5, pp. 613-620
[17] D'Orazio, A., *et al*., Application to Natural Convection Enclosed Flows of a Lattice Boltzmann BGK Model Coupled with a General Purpose Thermal Boundary Condition, *International Journal of Thermal Sciences*, *43* (2004), 6, pp. 575-586
[18] Shu, C., *et al*., Simulation of Natural Convection in a Square Cavity by Taylor Series Expansion and Least Squares-Based Lattice Boltzmann Method, *International Journal of Modern Physics*, *13* (2002), 10, pp. 1399-1414
[19] Moparthi, A., *et al*., Optimization of Heat Fluxes on the Heater and the Design Surfaces of a Radiating-Conducting Medium, *Numerical Heat Transfer*, *56* (2009), 10, pp. 846-860
[20] Ajith, M., *et al*., Boundary Surface Heat Fluxes in a Square Enclosure with an Embedded Design Element, *Journal of Thermophysics and Heat Transfer*, *24* (2010), 4, pp. 845- 849
[21] Das, R. *et al.*, An Inverse Analysis for Parameter Estimation Applied to a Non-Fourier Conduction-Radiation Problem, *Heat Transfer Engineering*, *32* (2011), 6, pp. 455-466
[22] Xie, J., Yuan, C., Parametric Study of Ice Thermal Storage System with Thin Layer Ring by Taguchi Method, *Applied Thermal Engineering*, *98* (2016), Apr., pp. 246-255
[23] Kim, K. D., *et al.*, Optimization of Parameters for the Synthesis of Zinc Oxide Nanoparticles by Taguchi Robust Design Method, *Colloids Surf. A Physicochem. Eng. Asp.*, *311* (2007), 1-3, pp.170-173
[24] Huang, C. N., Yu, C. C., Integration of Taguchi's Method and Multiple-Input, Multiple-Output ANFIS Inverse Model for the Optimal Design of a Water-Cooled Condenser, *Applied Thermal Engineering*, *98* (2016), pp. 605-609

[25] Nourgaliev, R. R., *et al*., The Lattice Boltzmann Equation Method: Theoretical Interpretation, Numerics and Implications*, International Journal of Multiphase Flow*, *29* (2003), 1, pp. 117-169

[26] Mezrhab, A., *et al.*, Lattice Boltzmann Modeling of Natural Convection in an Inclined Square Enclosure with Partitions Attached to its Cold Wall, *International Journal of Heat of Fluid Flow*, *27* (2006), 3, pp. 456-465

[27] Xuan, Y., Roetzel, W., Conceptions for Heat Transfer Correlation of Nanofluids, *Int. J. Heat Mass Transf.*, *43* (2000), 19, pp. 3701-3707

[28] Abu-Nada, E., *et al*., Natural Convection Heat Transfer Enhancement in Horizontal Concentric Annuli Using Nanofluids, *Int. Commun. Heat Mass*, *35* (2008), 5, pp. 657-665

[29] Chon, C. H., *et al.*, Empirical Correlation Finding the Role of Temperature and Particle Size for Nanofluid (Al_2O_3) Thermal Conductivity Enhancement, *Appl. Phys. Lett.*, *87* (2005), 15, 153107

[30] Minsta, A. H., *et al*., New Temperature and Conductivity Data for Water-Based Nanofluids, *Int. J. Therm. Sci.*, *48* (2009), 2, pp. 363-371

[31] Du, R., Liu, W., A New Multiple-Relaxation-Time Lattice Boltzmann Method for Natural Convection, *J. Sci. Comput*., *56* (2013), 1, pp. 122-130

[32] Dixit, H., Babu, V., Simulation of High Rayleigh Number Natural Convection in a Square Cavity Using the Tattice Boltzmann Method, *International Journal of Heat and Mass Transfer*, *49* (2006), 3-4, pp. 727-739

[33] Barakos, G., Mitsoulis, E., Natural Convection Flow in a Square Cavity Revisited: Laminar and Turbulent Models with Wall Functions, *International Journal for numerical methods in fluids*, *18* (1994), 7, pp. 695-719

[34] Bocu, Z., Altac, Z., Laminar Natural Convection Heat Transfer and Air Fow in Three-Dimensional Rectangular Enclosures with Pin Arrays Attached to Hot Wall, *Applied Thermal Engineering*, *31* (2011), 16, pp. 3189-3195

[35] Alinejad, J., Fallah, K., Taguchi Optimization Approach for Three-Dimensional Nanofluid Natural Convection in a Transformable Enclosure, *Journal of Thermophysics and Heat Transfer*, *31* (2017), 1, pp. 211-217

[36] Alinejad, J., Esfahani, J. A., Taguchi Design of Three Dimensional Simulations for Optimization of Turbulent Mixed Convection in a Cavity, *Meccanica*, *52* (2017), 4-5, pp. 925-938

Paper submitted: May 9, 2017
Paper revised: October 12, 2017
Paper accepted: October 29, 2017